Journal of Biomechanics 86 (2019) 79–88

Contents lists available at ScienceDirect

Journal of Biomechanics

journal homepage: www.elsevier.com/locate/jbiomech
www.JBiomech.com

Dynamic effect of beta-amyloid 42 on cell mechanics

Qi Gao [a,b], Yuqiang Fang [c], Shiqing Zhang [d], Ho Sze Hersey Wong [a], Yee Edward Chan [a], Samantha Sze Man Wong [d], Ken K.L. Yung [d], King W.C. Lai [a,b,*]

[a] Department of Biomedical Engineering, City University of Hong Kong, Kowloon, Hong Kong
[b] Centre for Robotics and Automation, City University of Hong Kong, Kowloon, Hong Kong
[c] Department of Engineering Mechanics, Jilin University, Changchun, China
[d] Department of Biology, Hong Kong Baptist University, Kowloon, Hong Kong

ARTICLE INFO

Article history:
Accepted 24 January 2019

Keywords:
Cell mechanics
AFM
Aβ1-42 oligomer

ABSTRACT

$A\beta_{1-42}$, which is highly toxic to neural cells, is commonly present in the brains of people with Alzheimer's disease. In this study, dynamic changes in cell mechanics were monitored under Aβ-induced toxicity. To investigate the changes in cellular mechanical properties, we used $A\beta_{1-42}$ oligomer at different concentrations to treat human neuroblastoma SH-SY5H cells. Results demonstrated a two-stage dynamic change in cell mechanics during neurodegeneration. Additionally, Young's modulus (YM) of the treated cells increased in a short period. The reasons include alteration in surface tension, osmotic pressure, and actin polymerization. Rough cellular membranes were observed from atomic force microscope (AFM) measurement. However, the cellular YM gradually decreased when the cells were continuously exposed to $A\beta_{1-42}$ or to a high concentration of $A\beta_{1-42}$. The major reason for the decreased YM was microtubule disassembly. Dynamic change in YM reflects different activities in cytoplasm in response to $A\beta_{1-42}$. The characteristic changes in cell mechanics provided insights into the dynamic neurodegeneration process of cells induced by $A\beta_{1-42}$ oligomer.

1. Introduction

Beta amyloid (Aβ), a major component of senile plaques, is present in the brains of patients with Alzheimer's disease (AD) and plays a crucial role in AD pathogenesis (Mattson, 2004) (Hardy and Selkoe, 2002). $A\beta_{1-42}$ contains 42 residues and is closely related to the pathogenesis of AD (Bhatia et al., 2000). $A\beta_{1-42}$ tends to convert from a native and soluble formation to an insoluble and aggregation statue aggregation, thereby further influencing cell viability. Formation ranges from monomer to other different forms including oligomer, protofibril, fibril, and plaque (Watanabe-nakayama et al., 2016). Although all amyloid forms were reported to alter cellular activity and induce neurotoxicity, recent studies demonstrated that amyloid toxicity is induced by the presence of oligomeric amyloids (Wang et al., 2016).

The aggregation and accumulation of $A\beta_{1-42}$ affect many cellular components, including plasma membrane and intracellular substances (Calamai et al., 2016) (Mokhtar et al., 2013). The Aβ oligomers interacted with potential receptors, such as integrin, and triggered endocytosis. Initialized Aβ was then transported to and degraded by the lysosomes (Verdier et al., 2004) (Zerbinatti and Bu, 2005). Furthermore, considerable efforts have been made for exploring the mechanism of $A\beta_{1-42}$ cytotoxicity (Lulevich et al., 2010). The hypothesis of exterior membrane damages induced by $A\beta_{1-42}$, such as membrane fragility and ion-channel formation, are proposed based on the investigation of lipid bilayer (Lal et al., 2007). In this dynamic process, $A\beta_{1-42}$ initially interacts with cell membrane, leading to changes of surface morphology (Lai and McLaurin, 2011), and further causes dysfunction of intracellular component (Reddy and Beal, 2008) (Mendoza-Naranjo and Gonzalez-Billault, 2007). The interior loss of ion homeostasis (Popugaeva et al., 2017) and cytoskeletal reorganization are well documented by previous studies that used the immunostaining based method (King et al., 2006). Cell stiffness, an essential property of biophysics, may be influenced by the $A\beta_{1-42}$ oligomer. Thus, understanding the Aβ-induced neurotoxicity is important. Nevertheless, various effects of Aβ on cell stiffness have been reported (Lulevich et al., 2010) (Ungureanu et al., 2016) (Canale et al., 2018), although the results are inconsistent with each other. In this regard, we aim to clarify the complex effect of $A\beta_{1-42}$ on cell mechanics. Several proposed pathways that tend to alter cellular mechanical properties are shown in Fig. 1. Our work focuses on dynamic changes in cellular YM during neurodegeneration.

* Corresponding author.
E-mail address: kinglai@cityu.edu.hk (K.W.C. Lai).

https://doi.org/10.1016/j.jbiomech.2019.01.046
0021-9290/

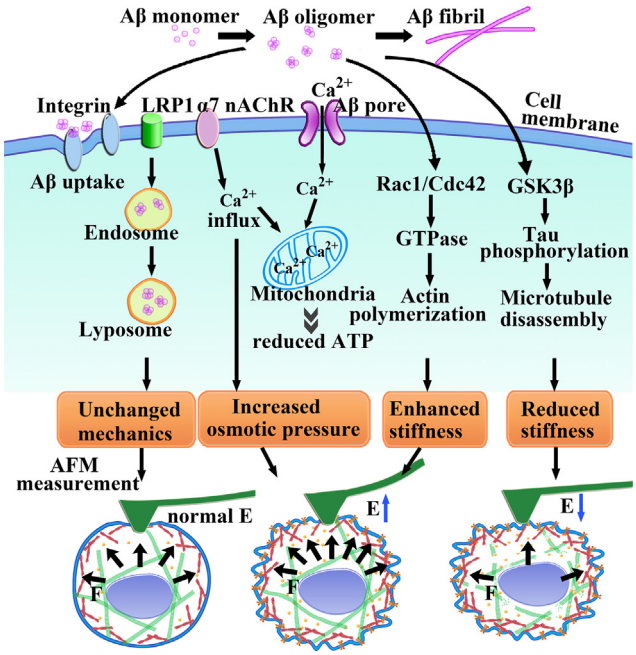

Fig. 1. Aβ associated pathways. It can be internalized or up taken by endocytosis. Calcium signaling caused by Aβ pore and receptor-mediated calcium influx results in high calcium concentration in cells. Aβ activates the Rac1/Cdc42 pathway and promotes actin polymerization, stimulates GSK3β, and triggers tau phosphorylation and microtubule disassembly.

In this study, cellular mechanics was recorded by AFM nanoindentation, which provides quantitative results. The results indicate a two-stage dynamic change of cell mechanics induced by $A\beta_{1\text{-}42}$ oligomer. We decomposed it into two phases: increased YM at the beginning and reduced value with prolonged time or enhanced concentration. Variations in surface tension, osmotic pressure, and actin polymerization are the possible reasons for the increased YM. AFM imaging proved that the surface of SH-SY5Y cells became rougher owing to the treatment of $A\beta_{1\text{-}42}$ oligomers. Nevertheless, the cellular YM declined afterward because the degeneration of cytoskeletal became a dominant factor. These results suggest a dynamic effect on YM during neurodegeneration induced by $A\beta_{1\text{-}42}$ oligomer and account for the prior opposite observation regarding the change in YM.

2. Materials and methods

2.1. $A\beta_{1\text{-}42}$ aggregation

Aβ power was purchased from Thermo Fisher Scientific. Lyophilized $A\beta_{1\text{-}42}$ powder was initially dissolved in Hanks' Balanced Salt Solution (HBSS) to obtain a concentration of 50 μM and incubated in an agitated water bath at 37 °C. We incubate the Aβ solution for 1 day and 4 days. Aβ oligomer can be found after 1 day of incubation, and the detail aggregation result is interpreted in the result section.

2.2. Cell culture and $A\beta_{1\text{-}42}$ treatment

Human neuroblastoma SH-SY5Y cells were cultured in complete medium, which contained DMEM/F12, supplemented with 10% fetal bovine serum and 1% antibiotic mixture (PSN) (Gibco). 50 μM $A\beta_{1\text{-}42}$ solution was incubated as described above. After 1 day of incubation, it was diluted by DMEM and applied to treat cells. SH-SY5Y cells were grown on coverslip and incubated in DMEM/F12, 250 nM, 750 nM, 1 μM, 2 μM and 5 μM $A\beta_{1\text{-}42}$ for 72-hour, respectively. In the following experiments, we utilized substrate-adherent cells and discard the floating cells during media changes. For AFM imaging, cells in different mediums were fixed by 4% paraformaldehyde (Sigma) for 30 mins.

2.3. AFM imaging

High-resolution imaging and nanoindentation were carried out by AFM detection system (BioScope Catalyst, Bruker Nano). An inverted optical microscope was mounted to the AFM system to posit cells and AFM probes in precise. Imaging of $A\beta_{1\text{-}42}$ aggregation was obtained by ScanAsyst fluid probe, while cell imaging was obtained by OLTESPA probe. Peak Force QNM mode was chosen to avoid tip contamination and minimize the interaction between AFM tip and biological samples, as well as to prevent samples from damaging. To obtain cell images using AFM, we fixed cells with 4% paraformaldehyde (PFA). We prepared 4% PFA in PBS solution firstly. Afterward, cells were incubated in 4% PFA for 30 mins in room temperature. Cells were washed with PBS solution for 3 times before measurement. With a tip radius < 7 nm, OLTESPA probe can help us to obtain a high-resolution image. The tip height is in the range of 9–19 μm, and the actual value of spring constant was calibrated using Sander method. In the scanning process, several scanning parameters were adjusted: scanning rate was set as 0.3 Hz, and image resolution was 256 * 256.

2.4. AFM nanoindentation

In nanoindentation experiments, contact mode in fluid was applied based on previously described (Fang et al., 2014). We treated cells with the Aβ oligomer for different time period (1-hour, 24-hour, 48-hour and 72-hour). After that, we rinsed sample with Hanks balance salt solution (HBSS) changed the medium to HBSS because the amino acid in culture medium affects measurement accuracy. Then, sample is mounted on to AFM stage. DNP-10 tips with V-shaped silicon nitride cantilever and pyramidal silicon nitride tip were applied to indent cells. The actual value of spring constant was calibrated using thermal tune method. The tip was moved at a velocity of 6 μm/s until a trigger force of 3 nN was reached. Sneddon model was chosen as the fit model to calculate the YM of the cells. The data portion with indentation depth ~600 nm was used. The half angle (α) of AFM tips was set as 18° while the Poisson ratio (ν) was set as 0.5. At each condition, at least 60 cells were tested to get a statistical analysis result. For each cell, approximately 25 force-distance curves were collected. The recording force-distance curves were fitted with:

$$F = \frac{2}{\pi}\frac{E}{1-\nu^2}\delta^2 \tan\alpha \quad (1)$$

where F is the loading force, E is YM and δ is the indentation depth.

2.5. Immunocytochemical detection of cytoskeleton

The organization of microtubule was detected by immunocytochemical method. Briefly, cells were fixed with 4% paraformaldehyde, and permeabilized with 0.2% of Triton X-100. Thereafter, slides were incubated with β-Tubulin rabbit antibody (CST-2128s, Cell Signaling) for 2-hour, followed by incubation with anti-rabbit IgG-Alexa Fluor 488 (Life Technology) for 1-hour at room temperature. Then, cells were observed under confocal microscope (SP8, Leica). Microtubule imaging was conducted at 488 nm laser excitation with emissions ranges of 490–550 nm.

2.6. Determination of P-tau by flow cytometry

Cells were resuspended in PBS, and fixed with 4% paraformaldehyde for 30 min. Then, cells were penetrated with 0.25% Triton-x100, and blocked by 5% BSA for 30 min at 4 . After that, cells were stained with anti-Phospho-Tau (Thr205) antibody (Cell Signaling). The secondary antibody was IgG-conjugated Alexa Fluor 488 (Life Technologies). Unstained was used as a control and to gate positive populations. Cells were analyzed on a BD FACSDiva Flow Cytometer (BD Biosciences).

2.7. Aβ toxicity assays

$A\beta_{1\text{-}42}$ induced cytotoxicity was evaluated using the lactate dehydrogenase (LDH) cytotoxicity assay and MTT assay. In the first case, SH-SY5Y cells were plated in 96-well microtiter plates. Culture medium was replaced by DMEM/F12 medium containing different concentration of $A\beta_{1\text{-}42}$. Based on the release of LDH form damaged cells, supernatant was collected to indicate neuronal injury. Measurements were following instruction of productive manufacturer. Briefly, 50 μl supernatant was mixed with reaction buffer for 30 min. Then, 50 μl of the stop solution was added to each well. Absorbance was read from a Spectra microplate reader. To determine the LDH activity, absorbance value at 680 nm was subtracted absorbance value at 490 nm. For the MTT assay, the cells were also cultured in 96-well plates. Then, they were treated with 5 μM $A\beta_{1\text{-}42}$ for 24 h. Afterward, each well was treated with 20 μl MTT solution (5 mg/ml), and incubated for another 4 h in 37 ℃ incubator. 150 μl Dimethyl sulfoxide (DMSO) was added to each well to dissolve Formazan deposition. Absorbance was read at 490 nm.

3. Results

3.1. Aβ oligomers induce inhomogeneous cellular Young's modulus

$A\beta_{1\text{-}42}$-derived cytotoxicity has been associated with the $A\beta_{1\text{-}42}$ aggregation. To evaluate $A\beta_{1\text{-}42}$ polymerization, we performed AFM imaging and continuously monitored the morphology changes. After 24-hour incubation, $A\beta_{1\text{-}42}$ oligomers, which were observed as globular aggregates, appeared to be the most dominant form, as shown in Fig. 1A. The results indicate that the diameter ranged from 3.0 nm to 5.6 nm, which was consistent with the result of a previous study (Mastrangelo et al., 2006). Quantitative analysis was performed on height distribution, and the results revealed that the mean height of $A\beta_{1\text{-}42}$ oligomer is 4.5 ± 0.7 nm ($n > 50$). To ensure the subsequent neurotoxicity study was entirely caused by $A\beta_{1\text{-}42}$ oligomers, $A\beta_{1\text{-}42}$ aggregation was monitored by AFM in an extended period of incubation. After 4 days, oligomer remained in the dominant structure. Only several short-length protofibrils were detected (Fig. 2B).

$A\beta_{1\text{-}42}$ oligomer (1 day of aggregation) was applied to treat cells. At a short treatment time (1-hour), the YM of SH-SY5Y cells treated with 5 μM $A\beta_{1\text{-}42}$ oligomer (1 day of aggregation) was higher than that of the control group. However, it declined in the 10 μM $A\beta_{1\text{-}42}$ group. Cellular YM demonstrated an opposite effect. A distinct trend is shown in Fig. 3. To connect intracellular activities with YM, we performed several time- and concentration-controlled experiments. These concentrations include 250 nM, 750 nM, 1 μM, 2 μM and 5 μM. They are defined as low, moderate, and high which have been described later.

3.2. Clearance of $A\beta_{1\text{-}42}$ without affecting mechanical property

For the detection of early cytotoxic events, the cells were exposed to $A\beta_{1\text{-}42}$ at a low concentration (250 nM). Changes in the YM were monitored for 72-hour as shown in Fig. 4A. Some fluctuations in the treated and the control groups were observed, and the difference between the groups was nonsignificant. We believe that this concentration is extremely low to cause further cytotoxicity. Growing evidence suggests that exogenous Aβ can be internalized with several types of Aβ-membrane interactions (Verdier et al., 2004) (Hu et al., 2009). Many membrane components may promote the formation of Aβ-receptor complexes and facilitate the uptake of these complexes by cells through receptor-mediated endocytosis. The examples of these receptors include low density lipoprotein receptor-like protein-1 (Lai and McLaurin, 2011) (Zerbinatti and Bu, 2005), α7 nicotinic acetylcholine receptor (α7nAChR) (Verdier et al., 2004) (Wang et al., 2000), and integrin (Verdier et al., 2004) (Bi et al., 2002). The interaction of Aβ with plasma membrane triggers this internalized process, called uptake pathway (Lai and McLaurin, 2011) (Chafekar et al., 2008). The $A\beta_{1\text{-}42}$ oligomers were uptaken by the SH-SY5Y cells via the endosome pathway and transported to the lysosomes. Finally, endocytosed $A\beta_{1\text{-}42}$ would be degraded in lysosomes, which was likely to attenuate its toxicity (Li et al., 2012) (Kanekiyo et al., 2013). Our experimental data revealed that clearance of $A\beta_{1\text{-}42}$ weakened cytotoxicity and caused minimal effect on the cell mechanics.

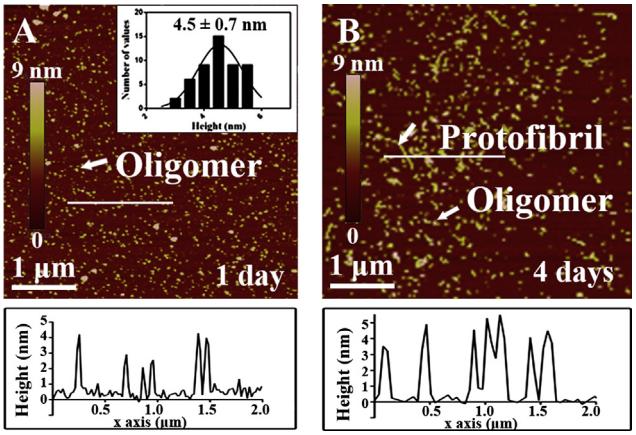

Fig. 2. AFM height images and height profile of $A\beta_{1\text{-}42}$ aggregation in HBSS after 1- and 4-day incubation. (A) $A\beta_{1\text{-}42}$ characterized as globular aggregations with height in the range of 3.0–5.6 nm. Histogram in (A) shows the mean height of $A\beta_{1\text{-}42}$ oligomer. (B) $A\beta_{1\text{-}42}$ characterized as globular oligomers with several protofibrils were scattered around them. Insets show height profile of $A\beta_{1\text{-}42}$. Scale bar: 1 μm.

3.3. Increased cellular stiffness resulted from moderate $A\beta_{1\text{-}42}$ exposure

Then, SH-SY5Y cells were treated with 750 nM $A\beta_{1\text{-}42}$ oligomers. Results are shown in Fig. 5A. With increased incubation time, the YM showed a rising trend. Statistical results reveal a significant increased value after 48-hour incubation. An extreme significance was observed after 72-hour treatment. Cellular YM increased from 1.5 kPa to 2.1 kPa. This observation suggests that a moderate concentration of $A\beta_{1\text{-}42}$ led to increased YM. To verify the relationship between $A\beta_{1\text{-}42}$ concentration and cellular mechanics, we further exposed cells to 1 μM $A\beta_{1\text{-}42}$. A similar change in trend in the first 24-hour was observed, as shown in Fig. 5B. Instead of the rising trend, the YM dropped when the treatment was longer than 24-hour. When the treatment time was extended to 72-hour, the YM of the experimental group reverted to the value of the control group, indicating that increase in the concentration of the $A\beta_{1\text{-}42}$ oligomer does not permanently increase cellular stiffness.

3.3.1. Alternation of membrane tension by $A\beta_{1\text{-}42}$ intercalation

Statistical analysis demonstrated that treated cells were stiffer than the control cells. The endosomal pathway was overwhelmed,

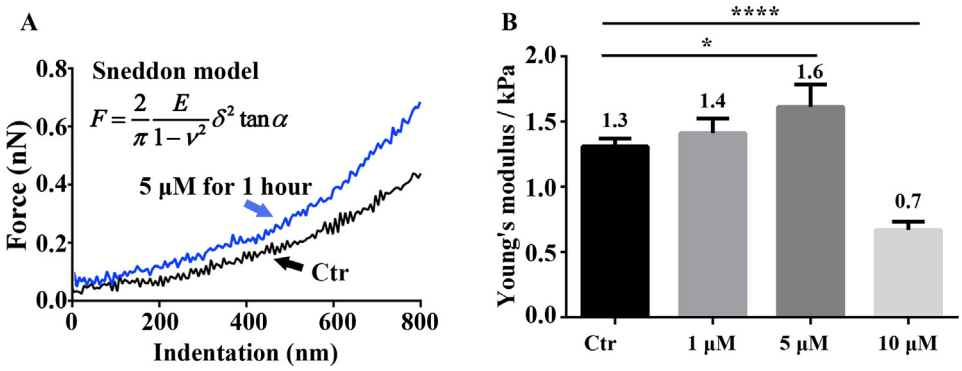

Fig. 3. (A) Representative force–distance curve obtained from AFM measurement. YM can be calculated after fitting with Sneddon model. (B) YM of SH-SY5Y cells exposed to $A\beta_{1\text{-}42}$ at different concentrations. The incubation time is 1-hour. $P < 0.05$ (*).

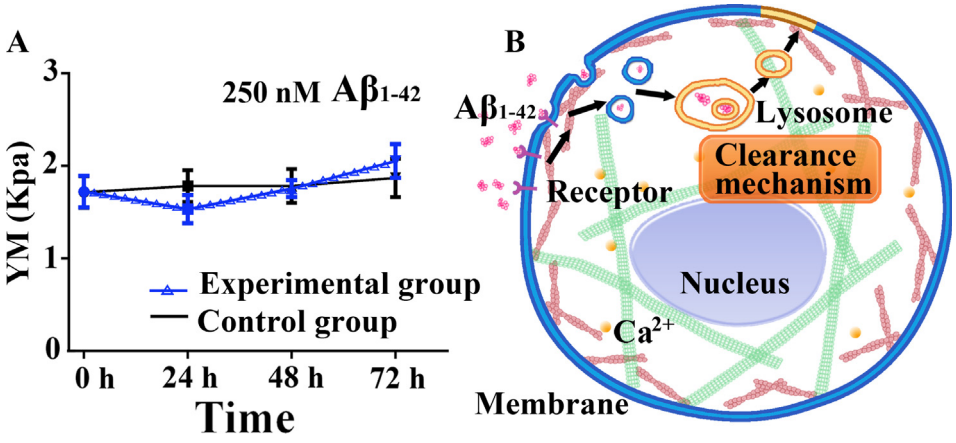

Fig. 4. (A) Variation of cellular YM with or without exposure to 250 nM $A\beta_{1\text{-}42}$. (B) Illustration of clearance mechanism of $A\beta_{1\text{-}42}$ at low physiologically relevant concentrations.

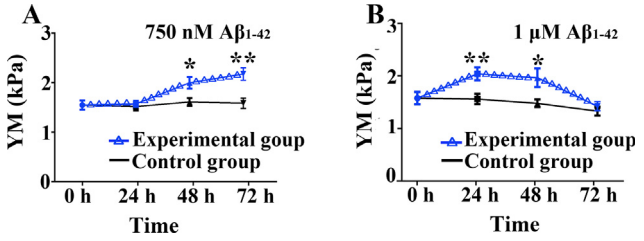

Fig. 5. Variation of cellular YM with or without exposure to 750 nM $A\beta_{1\text{-}42}$ (A) and 1 μM $A\beta_{1\text{-}42}$ (B). The asterisks indicate a statistically significant difference. $P < 0.05$ (*).

and downstream cytotoxicity pathways were triggered. The neurotoxic activities caused by $A\beta_{1\text{-}42}$ via several mechanisms have been proposed, namely, binding with membranes that cause membrane perturbations, significantly increasing ionic concentration (Oz et al., 2016), and following oxidative stress (Swomley et al., 2014). The secretion of $A\beta_{1\text{-}42}$ increases the likelihood of intercalation into the cellular membrane (Ding et al., 2012) (Chen et al., 2017) (Hong et al., 2014). Although the relationship of membrane tension involved in mechanical properties at the whole-cell level is unknown, plasma membrane with a high elastic modulus was reported (Hochmuth et al., 1973). Tension from plasma membrane helps regulate cell morphology physically. It is highly related with the force needed to deform cells (Diz-Muñoz et al., 2013). Sharing with similar way of amphipathic proteins which intercalate to membrane (Relini et al., 2014) (Seeliger et al., 2012), increased membrane tension occurred when $A\beta_{1\text{-}42}$ oligomer was added to the culture system. $A\beta_{1\text{-}42}$ interacted at the polar head of membrane, and the surface expansion produced a stress equivalent to a tension inside the membrane (Huang et al., 2004). Assuming that it is the sole factor response for the mechanics, surface tension (N) is proportional to the YM when the stress on the plane of the membrane is homogeneous. The YM of the cell membrane is given by Kamm (1986):

$$E_{tension} = N\frac{(1-\nu)}{\varepsilon h} \tag{2}$$

where ε is strain, $E_{tension}$ is YM, and h is the thickness of membrane. Thus, additional surface tension leads to an enhanced YM.

To verify $A\beta_{1\text{-}42}$ deformed cell membrane which increased YM, membrane structure was examined by AFM as shown in Fig. 6. Normal SH-SY5Y cells expressed a smooth surface. When cells presented in 250 nM $A\beta_{1\text{-}42}$ for 24-hour, no appreciable changes were observed. The results reveal that $A\beta_{1\text{-}42}$ has minimal toxic effect on membrane structure at a concentration of 250 nM. On the contrary, detectable perturbation or deformation of cell surface was be observed after exposure to a high concentration of $A\beta_{1\text{-}42}$. At $A\beta_{1\text{-}42}$ concentration of 750 nM, minor disruption in the membrane was observed after the 72-hour treatment. Similarly, a minor disruption was detected on the cells treated with 1 μM and 2 μM $A\beta_{1\text{-}42}$ for 24-hour. Moreover, the exposure of cells to 2 μM $A\beta_{1\text{-}42}$ for more than 48-hour led to serious surface perturbation. Disruptions in the membranes were also observed in the 5 μM group. According to these observations, we defined various conditions as low (250 nM), moderate (750 nM and 1 μM), and high (2 μM and

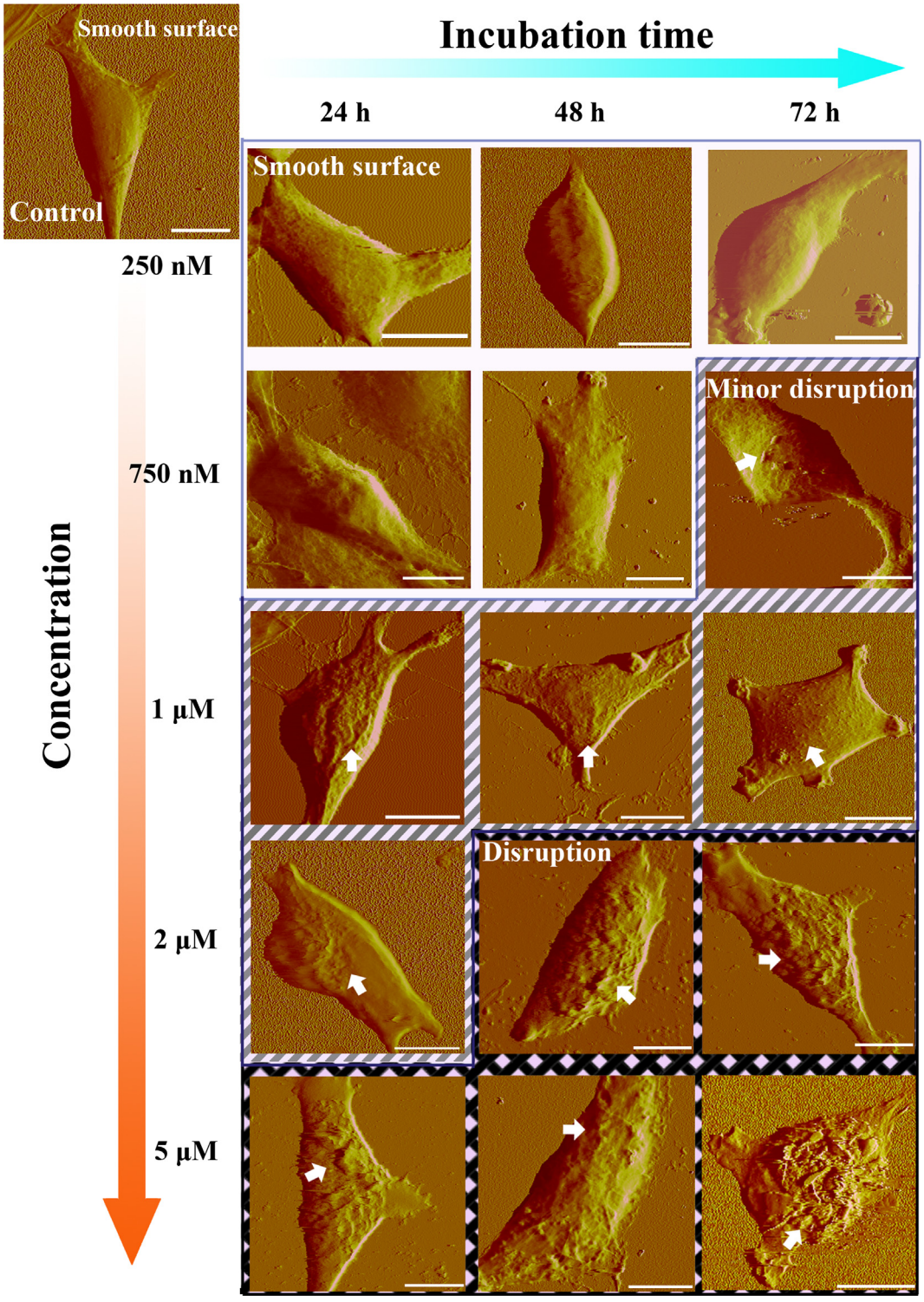

Fig. 6. AFM Peakforce images of control cell and cell incubated with $A\beta_{1\text{-}42}$ oligomer. Arrows indicate membrane disruption. Scale bar: 10 μm.

5 μM). Representative cellular morphology indicated the destructive effect of $A\beta_{1\text{-}42}$ on cell membranes. Multiple pathways are co-existed in the membrane disruption process. The peptide-lipid interaction occurred at the beginning initiates cell leakage and promotes Ca^{2+} influx. Besides, fusogenic caused by Aβ was also reported in prior researches (Vestergaard et al., 2013) (Akinlolu et al., 2015). Lipid mixing and vesicle fusion between liposomes have been suggested. Membrane structure provided direct evidence of $A\beta_{1\text{-}42}$-induced concentration-dependent changes.

3.3.2. Increased osmotic pressure by $A\beta_{1\text{-}42}$ induced calcium homeostasis

Another important factor is calcium homeostasis. Prior investigation revealed that specific Aβ channel-like structures form during the interaction of Aβ with the plasma membrane (Lal et al., 2007) (Lin et al., 2001). Moreover, the Ca^{2+}-uptake experiment provided an evidence that the channel-like structures have channel activity which facilitates cation transport (Jang et al., 2007). Aβ has also been shown to evoke an increasing of Ca^{2+} level via a

native receptor, such as α7-nAChRs (Oz et al., 2016). Above all, a series of studies indicated that the gain of intracellular calcium was highly related with cytotoxicity induced by Aβ (Oz et al., 2016) (Gunn et al., 2016) (Demuro and Parker, 2013). The imbalance of cytoplasmic Ca^{2+} causes ionic strength and subsequently enhances osmotic pressure because the overall concentration of intracellular Ca^{2+} is higher than that in control cells. The osmotic pressure of a dilute solution obeys the osmosis equation as follows:

$$\Delta\Pi = iMRT \tag{3}$$

where $\Delta\Pi$ is alternation of osmotic pressure, i is a dimensionless correction factor, M is molarity variation, R is gas constant, and T is temperature. The alternation of osmotic pressure increases the Bulk modulus (K) according to the following equation (Saito et al., 2006):

$$K = V\frac{\Delta P}{\Delta V} = V\frac{\Delta\Pi}{\Delta V} \tag{4}$$

where ΔP is alternation of pressure, and V is volume. Relationship between YM ($E_{osmotic}$) and K is:

$$E_{osmotic} = 3(1-2v)K = 3(1-2v)V\frac{\Delta\Pi}{\Delta V} \tag{5}$$

When osmotic pressure is the single reason for mechanics, rising intracellular ion concentration generates an increased osmotic pressure. Eqs. (4) and (5) show that variation in osmotic pressure increases the Bulk modulus and, subsequently, YM.

3.3.3. Actin polymerization due to enhanced Ca^{2+}

Another possibility is that enhanced Ca^{2+} induces actin polymerization (Mendoza-Naranjo and Gonzalez-Billault, 2007) (Park et al., 2016). These activities are Ca^{2+}-dependent mechanism. Actin polymerization subsequently works to increase local stiffness. The shear modulus (G) of actin network can be described as follows (Fleischer et al., 2007) (MacKintosh et al., 1995):

$$G \propto \frac{l_p^2}{l_e^3\xi^2} \tag{6}$$

where l_p is persistence length of actin filaments, l_e is length of entanglement actin, and ξ is mesh size.

Relationship between YM and shear modulus is given by:

$$E = \frac{G}{2(1+v)} \tag{7}$$

where ν is Poisson radio. Combining Eqs. (6) and (7), YM of actin network (E_{act}) can be found from:

$$E_{act} = \frac{G}{2(1+v_{act})} \propto \frac{l_p^2}{2(1+v_{act})l_e^3\xi^2} \tag{8}$$

Upon polymerization, the entanglement filaments and mesh size decreased. The shear modulus of the actin filaments is inversely proportional to length of entanglement actin filaments and mesh size (Fleischer et al., 2007) (MacKintosh et al., 1995). Thus, actin polymerization caused increased G, which yielded an increased E_{act} value from the given equation. Therefore, enhanced YM which resulted from actin polymerization can be obtained.

Membrane tension, osmotic pressure, and actin filaments had a positive effect on cell mechanics. Thus, an incremental YM could be deduced. The corresponding activities are shown in Fig. 7.

3.4. YM reduced dramatically after high-dose treatment

Subsequently, 2 μM $Aβ_{1-42}$ was used for the visualization of cellular YM. The results show that the YM of the treatment group initially exhibited rapid response (<24-hour), then dropped and showed less changes 48-hour later. At 72-hour, the value reduced

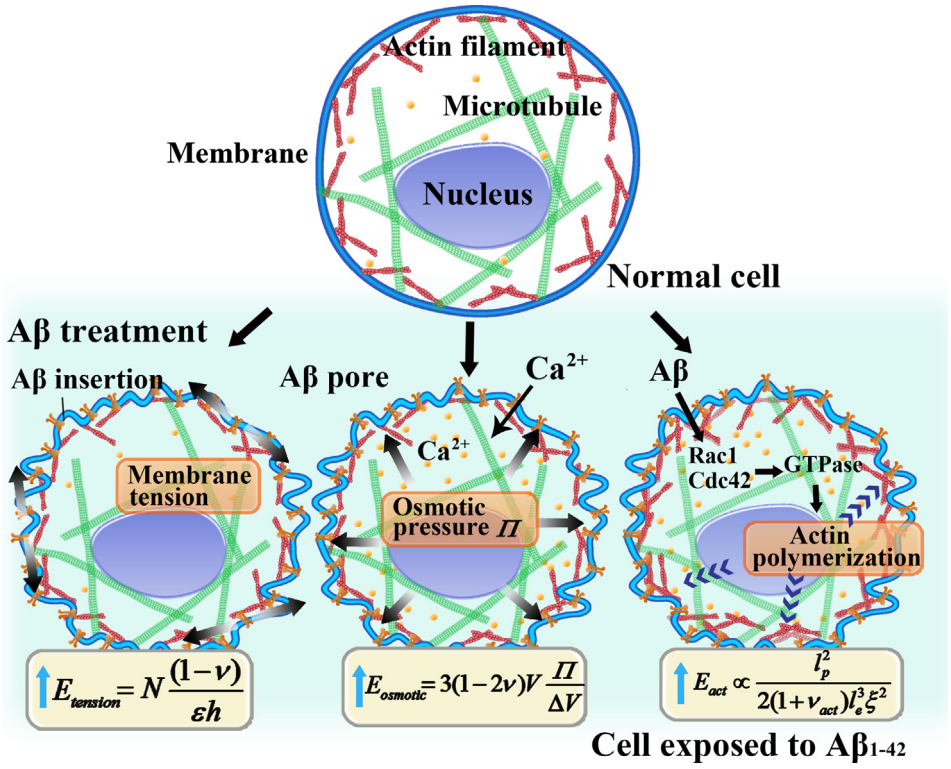

Fig. 7. Model of cell exposed to $Aβ_{1-42}$. Membrane folds are clearly visible after $Aβ_{1-42}$ intercalate to membrane. $Aβ_{1-42}$ forms ion channel and induces Ca^{2+} influx. Increased Ca^{2+} promotes actin polymerization in neurons.

to the value of control group, as shown in Fig. 8A. To accelerate $A\beta_{1-42}$-induced neurodegeneration and study the subsequent mechanism, we further exposed cells to 5 μM $A\beta_{1-42}$ as shown in Fig. 8B. Apart from the slight increase, no significant effect was observed for the first 24-hour. The treatment group decreased 24-hour later. The YM of the experimental group was much lower than the control group when the incubation time was extended to 48-hour. The SH-SY5Y cells demonstrated a time-dependent decrease in their YM during the test period. After the 72-hour incubation, the minimum YM was obtained, decreasing from 1.7 kPa to 1.3 kPa. A significant difference between the experimental and control groups was observed.

The result of the experiment on cell stiffness was contrary to our expectation. We considered the result as a second stage of changed cell mechanics. We speculate that the reduced YM could be a consequence of cytoskeleton rearrangement induced by $A\beta_{1-42}$ oligomers in neural cells. As the stiffest of the three types of cytoskeleton (Lopez and Valentine, 2015) (Fletcher and Mullins, 2010), disruption of microtubules could be in response to the decline of YM. $A\beta_{1-42}$ was reported to cause tau protein phosphorylation via activation of α7-nAChR (Oz et al., 2016). Phosphorylation of tau protein at multiple sites was detected by specific phosphor anti-tau antibodies (Zempel et al., 2010). This abnormally phosphorylated tau no longer stabilized microtubule and promoted microtubule disassembly. Aβ oligomers which caused tau phosphorylation and further loss of microtubule binding are shown in Fig. 8C. Mechanical properties of microtubule can be described by the length-dependent YM (E_{MT}) (Sept and MacKintosh, 2010) (Hawkins et al., 2013):

$$E_{MT} = \frac{l_{MT} k_B T}{\frac{\pi}{4}(R_{out}^4 - R_{in}^4)} \tag{9}$$

where E_{MT} is the YM of microtubule, k_B is Boltzmann's constant; R_{in} and R_{out} are the tube's internal and external diameters, respectively; and l_{MT} is persistence length of microtubule. Disassembled microtubules represent shorter length, which means YM reduced after high-concentration treatment.

Decreases in the YM of the cells exposed to high concentrations of $A\beta_{1-42}$ was observed. Previous studies reported that $A\beta_{1-42}$ causes tau phosphorylation, which in turn leads to microtubule disassembly (Fletcher and Mullins, 2010). To investigate the intracellular mechanism, we characterized immunofluorescence of the microtubules in the SH-SY5H cells and examined the specific effect of $A\beta_{1-42}$ oligomer on the cytoskeletons at different concentrations. The microtubule organization in the SH-SY5Y cells incubated with various concentrations of $A\beta_{1-42}$ for 72-hour exhibited different degrees of disassembly, as shown in Fig. 9A. Less organized microtubules were observed after long-time incubation or exposure to high concentrations of $A\beta_{1-42}$ oligomers. Changes of phosphorylated Tau was observed as shown in Fig. 9B. An increased fluorescence signal was observed in cells treated with 5 μM $A\beta_{1-42}$ oligomer for 72 h.

3.5. Validation of $A\beta_{1-42}$ induced cytotoxicity

To characterize the cytotoxicity further, we determined LDH release in the culture medium. Fig. 10 displays the effects of $A\beta_{1-42}$ oligomers on cell viability in an exposure-time-dependent manner. A concentration of 250 nM $A\beta_{1-42}$ had no significant effect during the incubation period. However, the addition of micromolar $A\beta_{1-42}$ to the SH-SY5Y cells increased LDH release, which indicated a high cytotoxicity. Following 48-hour exposure of the cells with $A\beta_{1-42}$, a major increase in LDH level was observed in the treatment groups (750 nM, 1 μM, 2 μM, and 5 μM). Statistical analysis

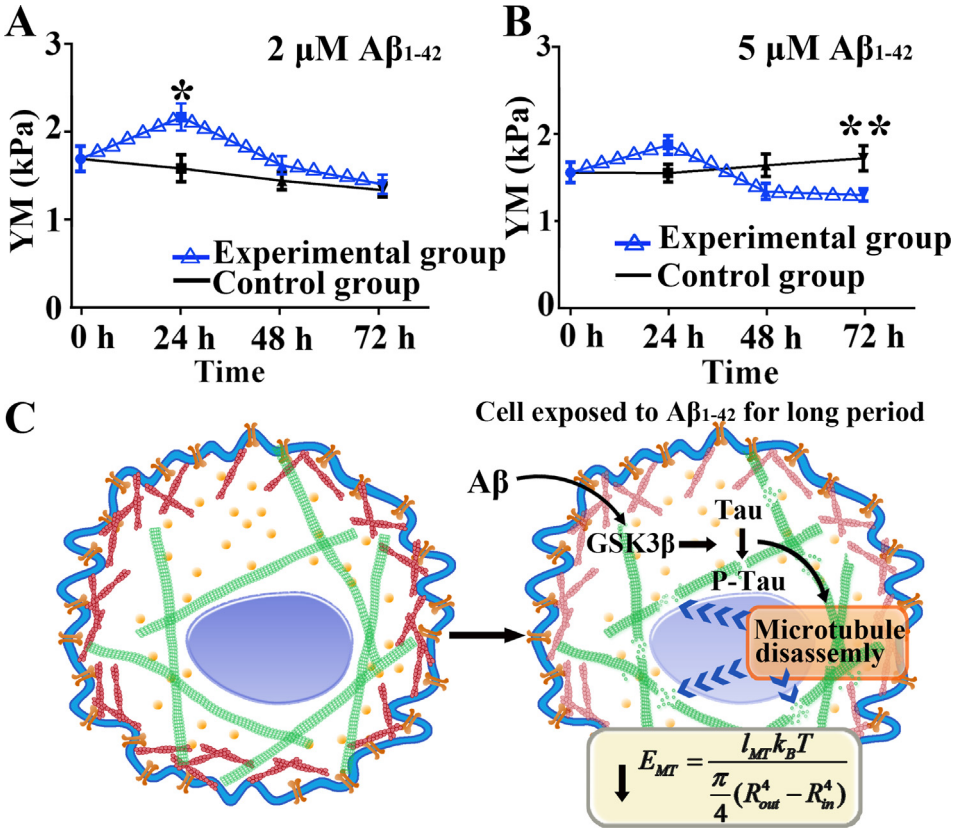

Fig. 8. Variation of cellular YM exposure to 2 μM $A\beta_{1-42}$ (A) and 5 μM (B). $P < 0.05$ (*) (C) $A\beta_{1-42}$ promoted microtubule disassembly after a long incubation time.

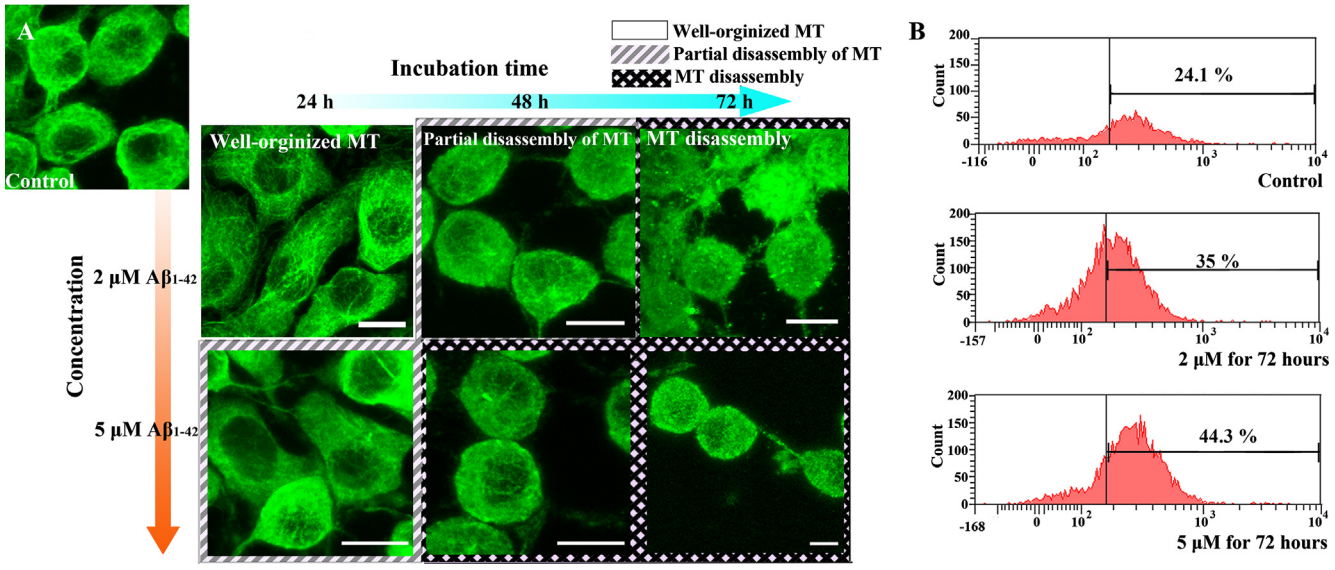

Fig. 9. (A) Representative immunostains of microtubules in normal SH-SY5Y cells. Immunofluorescence images show microtubules disordered after treatment with 2 μM and 5 μM $A\beta_{1\text{-}42}$ oligomers. Less organized microtubules are observed in treated cells. Scale bar: 10 μm. (B) Level of phosphorylated Tau increased when treated with 2 μM and 5 μM $A\beta_{1\text{-}42}$ oligomer. Histograms of count versus Alexa Fluor 488 fluorescence.

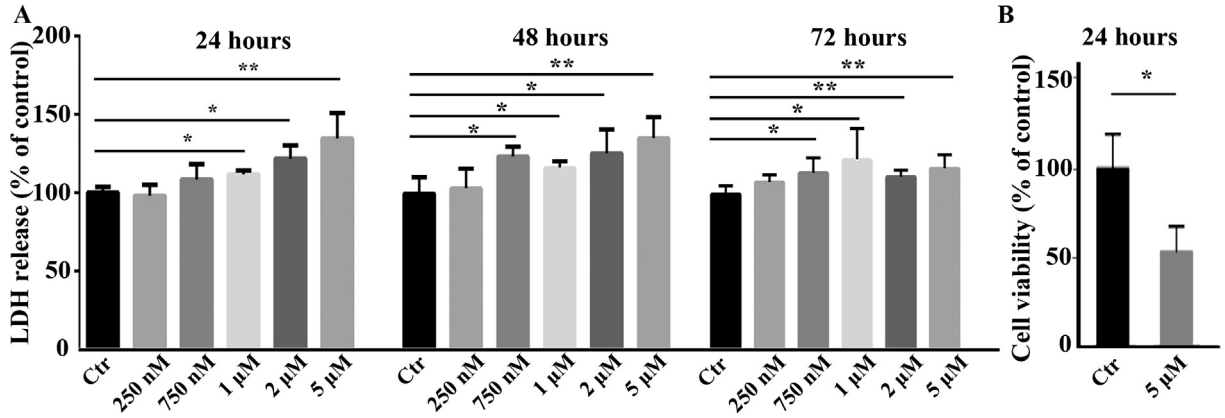

Fig. 10. Toxicity of $A\beta_{1\text{-}42}$ oligomer on SH-SY5Y cells. (A) Relevant LDH release is demonstrated. Values represent mean ± SD (*p < 0.05). (B) The results of MTT assay revealed that cells exposed to 5 μM $A\beta_{1\text{-}42}$ oligomer for 24-hour decreased cell viability.

revealed significant cell death at this stage. Similarly, after the 72-hour exposure, the cells treated with $A\beta_{1\text{-}42}$ significantly lost their viability. Microtubule disassembly was associated with apoptosis. The LDH level in medium was elevated for 72-hour. Results nearly supported the reduction of YM. Consistent with these results, the effect of $A\beta_{1\text{-}42}$ on cell activities was closely related with YM. Cell viability was also estimated using an MTT assay. Since 5 μM $A\beta_{1\text{-}42}$ influence LDH level significant after 24-hour, we used MTT assay to verify cell viability at this condition. It suggested that 5 μM $A\beta_{1\text{-}42}$ oligomer showed distinct cytotoxicity (* $P < 0.05$).

Cell responses to the addition of $A\beta_{1\text{-}42}$ show a time-course process owing to the complex biological system. Responses of neural cells to $A\beta_{1\text{-}42}$ oligomers were accompanied by the disturbances in their plasma membranes, including Ca^{2+} elevation, tau phosphorylation, and microtubule loss. These reactions altered the cellular mechanical properties in varying degrees and led to a combined effect. Previous studies demonstrated increased cellular stiffness after $A\beta_{1\text{-}42}$ treatment (Lulevich et al., 2010), whereas others showed decreased membrane stiffness (Ungureanu et al., 2016). To clarify the effects, time- and concentration-dependent experiments were performed here. A two-stage dynamic change provided a detailed response in $A\beta_{1\text{-}42}$ oligomer-induced cytotoxicity and explained prior opposite results. These observations suggested that fluctuation in YM was a comprehensive result. Mechanical responses provided new insights into $A\beta_{1\text{-}42}$ oligomer cytotoxicity.

4. Conclusions

We investigate the dynamic behaviour of $A\beta_{1\text{-}42}$ oligomer on the mechanical properties of neural cells. The characteristics of the cellular YM at different stages are employed by AFM-based nanoindentation. A small amount of $A\beta_{1\text{-}42}$ oligomer has minimal effect on cells despite long incubation time. The YM increased gradually as the concentration increased. However, continuous increase in $A\beta_{1\text{-}42}$ concentration or continuous exposure to $A\beta_{1\text{-}42}$ for a long period decreased the YM. This transient response suggests that $A\beta_{1\text{-}42}$ oligomers trigger multiple pathways. Our results show that changes in cellular mechanical properties can reflect the dynamic effect of $A\beta_{1\text{-}42}$ oligomers in the neurodegeneration process. Identification of this two-stage dynamic process explained the inconsistent of previous findings. These features reveal an effect of $A\beta_{1\text{-}42}$ induced cytotoxicity on cell mechanics.

Acknowledgements

The research was supported by grants from GRF grant from the Research Grant Council of the Hong Kong Special Administrative Region Government (CityU11205514 and CityU11205815).

Conflict of interests

The authors declare that they have no conflict of interest.

References

Akinlolu, R.D., Nam, M., Qiang, W., 2015. Competition between fibrillation and induction of vesicle fusion for the membrane-associated 40-residue β-amyloid peptides. Biochemistry 54 (22), 3416–3419. https://doi.org/10.1021/acs.biochem.5b00321.

Bhatia, R., Lin, H., Lal, R., 2000. Fresh and globular amyloid beta protein (1–42) induces rapid cellular degeneration: evidence for AbetaP channel-mediated cellular toxicity. FASEB J. 14 (9), 1233–1243. https://doi.org/10.1096/fasebj.14.9.1233.

Bi, X., Gall, Ã.C.M., Zhou, J., Lynch, G., 2002. Uptake and pathogenic effects of amyloid beta peptide 1–42 are enhanced by integrin antagonists and blocked by NMDA receptor antagonists. Neuroscience 112 (4), 827–840.

Calamai, M., Evangelisti, E., Cascella, R., Parenti, N., Cecchi, C., Stefani, M., Pavone, F., 2016. Single molecule experiments emphasize GM1 as a key player of the different cytotoxicity of structurally distinct Aβ1–42 oligomers. *Biochimica et Biophysica Acta (BBA)*- Biomembranes 1858 (2), 386–392. https://doi.org/10.1016/j.bbamem.2015.12.009.

Canale, C., Oropesa-Nuñez, R., Diaspro, A., Dante, S., 2018. Amyloid and membrane complexity: The toxic interplay revealed by AFM. Semin. Cell Dev. Biol. 73, 82–94 https://doi.org/10.1016/j.semcdb.2017.08.046.

Chafekar, S.M., Baas, F., Scheper, W., 2008. Oligomer-specific Aβ toxicity in cell models is mediated by selective uptake. Biochim. et Biophys. Acta – Mol. Basis Dis. 1782 (9), 523–531. https://doi.org/10.1016/j.bbadis.2008.06.003.

Chen, G., Xu, T., Yan, Y., Zhou, Y., Jiang, Y., Melcher, K., Xu, H.E., 2017. Amyloid beta: structure, biology and structure-based therapeutic development. Acta Pharmacol. Sin. 38, 1205. https://doi.org/10.1038/aps.2017.28.

Demuro, A., Parker, I., 2013. Cytotoxicity of intracellular aβ42 amyloid oligomers involves Ca2+ release from the endoplasmic reticulum by stimulated production of inositol trisphosphate. J. Neurosci.: Off. J. Soc. Neurosci. 33 (9), 3824–3833. https://doi.org/10.1523/JNEUROSCI.4367-12.2013.

Ding, H., Schauerte, J.A., Steel, D.G., Gafni, A., 2012. β-Amyloid (1–40) peptide interactions with supported phospholipid membranes: a single-molecule study. Biophys. J . 103 (7), 1500–1509. https://doi.org/10.1016/j.bpj.2012.08.051.

Diz-Muñoz, A., Fletcher, D.A., Weiner, O.D., 2013. Use the force: Membrane tension as an organizer of cell shape and motility. Trends Cell Biol. 23 (2), 47–53. https://doi.org/10.1016/j.tcb.2012.09.006.

Fang, Y., Iu, C.Y.Y., Lui, C.N.P., Zou, Y., Fung, C.K.M., Li, H.W., Lai, K.W.C., 2014. Investigating dynamic structural and mechanical changes of neuroblastoma cells associated with glutamate-mediated neurodegeneration. Sci. Rep. 4, 7074. https://doi.org/10.1038/srep07074.

Fleischer, F., Ananthakrishnan, R., Eckel, S., Schmidt, H., Käs, J., Svitkina, T., Beil, M., 2007. Actin network architecture and elasticity in lamellipodia of melanoma cells. New J. Phys. 9 (11), 420. https://doi.org/10.1088/1367-2630/9/11/420.

Fletcher, D.A., Mullins, R.D., 2010. Cell mechanics and the cytoskeleton. Nature 463 (7280), 485–492. https://doi.org/10.1038/nature08908.

Gunn, A.P., Wong, B.X., Johanssen, T., Griffith, J.C., Masters, C.L., Bush, A.I., Cherny, R. A., 2016. Amyloid-β peptide Aβ3pE-42 induces lipid peroxidation, membrane permeabilization, and calcium influx in neurons. J. Biol. Chem. 291 (12), 6134–6145. https://doi.org/10.1074/jbc.M115.655183.

Hardy, J., Selkoe, D.J., 2002. The amyloid hypothesis of Alzheimer's disease: progress and problems on the road to therapeutics. Science 297 (5580), 353–356. https://doi.org/10.1126/science.1072994.

Hawkins, T.L., Sept, D., Mogessie, B., Straube, A., Ross, J.L., 2013. Mechanical properties of doubly stabilized microtubule filaments. Biophys. J. 104 (7), 1517–1528. https://doi.org/10.1016/j.bpj.2013.02.026.

Hochmuth, R.M., Mohandas, N., Blackshear, P.L., 1973. Measurement of the elastic modulus for red cell membrane using a fluid mechanical technique. Biophys. J . 13 (8), 747–762. https://doi.org/10.1016/S0006-3495(73)86021-7.

Hong, S., Ostaszewski, B.L., Yang, T., O'Malley, T.T., Jin, M., Yanagisawa, K., Selkoe, D. J., 2014. Soluble Aβ oligomers are rapidly sequestered from brain ISF in vivo and bind GM1 ganglioside on cellular membranes. Neuron 82 (2), 308–319. https://doi.org/10.1016/j.neuron.2014.02.027.

Hu, X., Crick, S.L., Bu, G., Frieden, C., Pappu, R.V., Lee, J.-M., 2009. Amyloid seeds formed by cellular uptake, concentration, and aggregation of the amyloid-beta peptide. Proc. Natl. Acad. Sci. 106 (48), 20324–20329. https://doi.org/10.1073/pnas.0911281106.

Huang, H.W., Chen, F.Y., Lee, M.T., 2004. Molecular mechanism of peptide-induced pores in membranes. Phys. Rev. Lett. 92 (19), 198304–1198301. https://doi.org/10.1103/PhysRevLett. 92.198304.

Jang, H., Zheng, J., Nussinov, R., 2007. Models of β-amyloid ion channels in the membrane suggest that channel formation in the bilayer is a dynamic process. Biophys. J. 93 (6), 1938–1949. https://doi.org/10.1529/biophysj.107.110148.

Kamm, R.D., 1986. Cell membrane mechanics and adhesion.

Kanekiyo, T., Cirrito, J.R., Liu, C.-C., Shinohara, M., Li, J., Schuler, D.R., Bu, G., 2013. Neuronal clearance of amyloid-β by endocytic receptor LRP1. J. Neurosci. 33 (49), 19276–19283. https://doi.org/10.1523/JNEUROSCI.3487-13.2013.

King, M.E., Kan, H.M., Baas, P.W., Erisir, A., Glabe, C.G., Bloom, G.S., 2006. Tau-dependent microtubule disassembly initiated by prefibrillar beta-amyloid. J. Cell Biol. 175 (4), 541–546. https://doi.org/10.1083/jcb.200605187.

Lai, A.Y., McLaurin, J., 2011. Mechanisms of amyloid-beta peptide uptake by neurons: the role of lipid rafts and lipid raft-associated proteins. Int. J. Alzheimer's Dis. 2011, 1–11. https://doi.org/10.4061/2011/548380.

Lal, R., Lin, H., Quist, A.P., 2007. Amyloid beta ion channel : 3D structure and relevance to amyloid channel paradigm. Biochim. et Biophys. Acta (BBA)-Biomembr. 1768 (8), 1966–1975. https://doi.org/10.1016/j.bbamem.2007.04.021.

Li, J., Kanekiyo, T., Shinohara, M., Zhang, Y., LaDu, M.J., Xu, H., Bu, G., 2012. Differential regulation of amyloid-β endocytic trafficking and lysosomal degradation by apolipoprotein E isoforms. J. Biol. Chem. 287 (53), 44593–44601. https://doi.org/10.1074/jbc.M112.420224.

Lin, H.a.I., Bhatia, R., Lal, R., 2001. Amyloid β protein forms ion channels: implications for Alzheimer's disease pathophysiology. FASEB J. 15 (13), 2433–2444. https://doi.org/10.1096/fj.01-0377com.

Lopez, B.J., Valentine, M.T., 2015. Molecular control of stress transmission in the microtubule cytoskeleton. Biochim. et Biophys. Acta – Mol. Cell Res. 1853 (11), 3015–3024. https://doi.org/10.1016/j.bbamcr.2015.07.016.

Lulevich, V., Zimmer, C.C., Hong, H.-S., Jin, L.-W., Liu, G.-Y., 2010. Single-cell mechanics provides a sensitive and quantitative means for probing amyloid-β peptide and neuronal cell interactions. Proc. Natl. Acad. Sci. 107 (31), 13872–13877. https://doi.org/10.1073/pnas.1008341107.

MacKintosh, F.C., Käs, J., Janmey, P.A., 1995. Elasticity of semiflexible biopolymer networks. Phys. Rev. Lett. 75 (24), 4425–4429. https://doi.org/10.1103/PhysRevLett. 75.4425.

Mastrangelo, I.a., Ahmed, M., Sato, T., Liu, W., Wang, C., Hough, P., Smith, S.O., 2006. High-resolution Atomic Force Microscopy of Soluble Aβ42 Oligomers. J. Mol. Biol. 358 (1), 106–119. https://doi.org/10.1016/j.jmb.2006.01.042.

Mattson, M.P., 2004. Pathways towards and away from Alzheimer's disease. Nature 430 (7000), 631–639. https://doi.org/10.1038/nature02940.

Mendoza-Naranjo, A., Gonzalez-Billault, C.M.R., 2007. Aβ1-42 stimulates actin polymerization in hippocampal neurons through Rac1 and Cdc42 Rho GTPases. J. Cell Sci. 120 (2), 279–288. https://doi.org/10.1242/jcs.03323.

Mokhtar, S.H., Bakhuraysah, M.M., Cram, D.S., Petratos, S., 2013. The beta-amyloid protein of Alzheimer's disease: communication breakdown by modifying the neuronal cytoskeleton. Int. J. Alzheimer's Dis. 2013. https://doi.org/10.1155/2013/910502.

Oz, M., Petroianu, G., Lorke, D.E., 2016. α7-nicotinic acetylcholine receptors: new therapeutic avenues in Alzheimer's disease. Nicotinic Acetylcholine Receptor Technologies. https://doi.org/10.1007/978-1-4939-3768-4-9.

Park, K.R., Kwon, M.-S., An, J.Y., Lee, J.-G., Youn, H.-S., Lee, Y., Eom, S.H., 2016. Structural implications of Ca(2+)-dependent actin-bundling function of human EFhd2/Swiprosin-1. Sci. Rep. 6, 39095. https://doi.org/10.1038/srep39095.

Popugaeva, E., Pchitskaya, E., Bezprozvanny, I., 2017. Dysregulation of neuronal calcium homeostasis in Alzheimer' s disease - A therapeutic opportunity? Biochem. Biophys. Res. Commun. 483 (4), 998–1004. https://doi.org/10.1016/j.bbrc.2016.09.053.

Reddy, P.H., Beal, M.F., 2008. Amyloid beta, mitochondrial dysfunction and synaptic damage: implications for cognitive decline in aging and Alzheimer's disease. Trends Mol. Med. 14 (2), 45–53. https://doi.org/10.1016/j.molmed.2007.12.002.

Relini, A., Marano, N., Gliozzi, A., 2014. Probing the interplay between amyloidogenic proteins and membranes using lipid monolayers and bilayers. Adv. Colloid Interface Sci. 207 (1), 81–92. https://doi.org/10.1016/j.cis.2013.10.015.

Saito, T., Soga, K., Hoson, T., Terashima, I., 2006. The bulk elastic modulus and the reversible properties of cell walls in developing Quercus leaves. Plant Cell Physiol. 47 (6), 715–725. https://doi.org/10.1093/pcp/pcj042.

Seeliger, J., Evers, F., Jeworrek, C., Kapoor, S., Weise, K., Andreetto, E., Winter, R., 2012. Cross-amyloid interaction of Aβ and IAPP at lipid membranes. Angew. Chemie – Int. Ed. 51 (3), 679–683. https://doi.org/10.1002/anie.201105877.

Sept, D., MacKintosh, F.C., 2010. Microtubule easticity: Connecting all-Atom simulations with continuum mechanics. Phys. Rev. Lett. 104 (1), 1–4. https://doi.org/10.1103/PhysRevLett. 104.018101.

Swomley, A.M., Förster, S., Keeney, J.T., Triplett, J., Zhang, Z., Sultana, R., Butterfield, D.A., 2014. Abeta, oxidative stress in Alzheimer disease: Evidence based on proteomics studies. Biochim. et Biophys. Acta – Mol. Basis Dis. 1842 (8), 1248–1257. https://doi.org/10.1016/j.bbadis.2013.09.015.

Ungureanu, A., Benilova, I., Krylychkina, O., Braeken, D., 2016. Amyloid beta oligomers induce neuronal elasticity changes in age-dependent manner: a force spectroscopy study on living hippocampal neurons. Sci. Rep. 6, 1–13. https://doi.org/10.1038/srep25841.

Verdier, Y., Zarándi, M., Penke, B., 2004. Amyloid β-peptide interactions with neuronal and glial cell plasma membrane: Binding sites and implications for Alzheimer's disease. J. Pept. Sci. 10 (5), 229–248. https://doi.org/10.1002/psc.573.

Vestergaard, M.C., Morita, M., Hamada, T., Takagi, M., 2013. Membrane fusion and vesicular transformation induced by Alzheimer's amyloid beta. Biochim. et

Biophys. Acta (BBA) – Biomembr. 1828 (4), 1314–1321. https://doi.org/10.1016/j.bbamem.2013.01.015.
Wang, H., Lee, D.H.S., Andrea, M.R.D., Peterson, P.a., Shank, R.P., Reitz, A.B., 2000. β-amyloid 1–42 binds to α7 nicotinic acetylcholine receptor with high affinity. J. Biol. Chem. 275 (8), 5626–5632. https://doi.org/10.1074/jbc.275.8.5626.
Wang, Z., Tan, L., Liu, J., Yu, J., 2016. The essential role of soluble A β oligomers in Alzheimer' s disease. Mol. Neurobiol. 53 (3), 1905–1924. https://doi.org/10.1007/s12035-015-9143-0.
Watanabe-nakayama, T., Ono, K., Itami, M., Takahashi, R., Teplow, D.B., 2016. High-speed atomic force microscopy reveals structural dynamics of amyloid β1–42 aggregates. Proc. Natl. Acad. Sci. 113 (21), 5835–5840. https://doi.org/10.1073/pnas.1524807113.
Zempel, H., Thies, E., Mandelkow, E., Mandelkow, E., 2010. Aβ oligomers cause localized Ca2+ elevation, missorting of endogenous tau into dendrites, tau phosphorylation, and destruction of microtubules and spines. J. Neurosci. 30 (36), 11938–11950. https://doi.org/10.1523/JNEUROSCI.2357-10.2010.
Zerbinatti, C.V., Bu, G., 2005. LRP and Alzheimer's disease. Rev. Neurosci. 135, 123–135. https://doi.org/10.1515/REVNEURO.2005.16.2.123.